Tolerance Investigation on a Helically Corrugated Interaction Circuit of a 265 GHz Gyro-TWA

Max Vöhringer, Alexander Marek, Stefan Illy, Benjamin Ell, Lukas Feuerstein, Gerd Gantenbein, Tobias Ruess, Chuanren Wu, Manfred Thumm, *Life Fellow, IEEE*, and John Jelonnek, *Senior Member, IEEE*

***Abstract*—Gyro-traveling-wave amplifiers (TWAs) with a helically corrugated interaction region (HCIR) are used for broadband, high-power amplification of microwave signals. In this publication, an HCIR for 265 GHz (G-band) and the influence of manufacturing tolerances on the HCIR performance are presented. This is done by using three different approaches. First, the influence of uniform deviations along the HCIR on the wave dispersion is considered. Second, particle in cell simulations for uniform deviations are conducted. Third, the influence of nonuniform randomly distributed manufacturing tolerances is investigated. It is found that uniform deviations along the HCIR strongly degrade gain and bandwidth, which results in small acceptable tolerances for these deviations. However, these constitute systematic errors, which can be compensated by adjusting the manufacturing process. In contrast, nonuniform deviations along the HCIR with Gaussian random distribution, e.g., caused by vibrations during manufacturing, do not exhibit the same characteristics. These are investigated by PIC simulation of HCIRs with random deviations along their outer wall. Their effect on gain and bandwidth has been shown to be smaller compared to uniform deviations, which allows for increased tolerances for nonuniform deviations.**

***Index Terms*—Broadband amplification, gyrotron-traveling-wave amplifier (TWA), helically corrugated waveguide.**

I. Introduction

HIGH-POWER broadband amplifiers in the G-band and above are currently discussed as microwave sources for future pulsed dynamic nuclear polarization (DNP) methods. DNP is a highly effective method for enhancing the performance of nuclear magnetic resonance (NMR). This technique leverages the electron magnetic moment, which is about 660 times larger than that of a proton [1], as opposed to the weaker nuclear magnetic moments used in conventional NMR. By coupling nuclear spins to highly polarized electrons, DNP-NMR dramatically boosts nuclear spin polarization, achieving increases of two to five orders of magnitude. As a result, experimental acquisition times can be reduced by up to a factor of 10^4 [2].

The key to DNP-NMR is the strong irradiation of the sample with high-power microwaves in the sub-terahertz range. For commercially available systems starting at an NMR frequency of 400 MHz, the corresponding microwave sources must operate at frequencies close to 263 GHz. Currently, most commercially available DNP-NMR systems employ a field-dependent continuous wave (CW) approach to transfer polarization from electrons to nuclei. However, coherent, pulsed polarization transfer [3] holds significant promise for more efficient polarization transfer. This method can enhance both the rate at which nuclear spins are polarized and the maximum achievable polarization. Pulsed DNP sequences, such as NOVEL [4] and TOP DNP [2], are active areas of research for high magnetic fields, with a demand for time-sequenced high-power microwave pulses up to 1 kW within a 15 GHz bandwidth at 265 GHz.

To produce coherent microwave pulses with sufficient power, high-power amplifiers are essential. Two promising amplifier designs are the dielectric-loaded gyro-traveling-wave amplifier (TWA) [5] and the helical gyro-TWA [6]. The dielectric-loaded gyro-TWA mitigates self-oscillations caused by internal feedback by incorporating lossy elements into the interaction circuit [7]. In contrast, the helical gyro-TWA enhances bandwidth and reduces sensitivity to velocity spreads in the electron beam by employing helical corrugations in the interaction circuit, referred to as the helically corrugated interaction region (HCIR). In addition, this design operates at the second harmonic, reducing the required static magnetic field by a factor of two. This reduction is particularly significant at higher frequencies around 265 GHz, where the static magnetic field decreases from 10 to 5 T. At this lower field, more cost-effective and easier-to-produce NbTi superconductors can be used instead of the Nb_3Sn superconductors typically required for 10 T magnets. Due to these advantages, this study focuses on the helical gyro-TWA. However, besides the previously mentioned advantages, there are also drawbacks. One disadvantage of the helical gyro-TWA is the more complex shape of the interaction circuit, which is discussed in the following section. This requires an advanced manufacturing process and

Received 29 November 2024; revised 26 March 2025; accepted 14 April 2025. This work was supported by Collaborative Research Centre 1527 "HyPERiON" through German Research Association Deutsche Forschungsgemeinschaft (DFG) under Grant SFB 1527. The review of this article was arranged by Senior Editor S. J. Gitomer. *(Corresponding author: Max Vöhringer.)*

Max Vöhringer, Manfred Thumm, and John Jelonnek are with the Institute of Radio Frequency Engineering and Electronics, Karlsruhe Institute of Technology, 76131 Karlsruhe, Germany, and also with the Institute for Pulsed Power and Microwave Technology, Karlsruhe Institute of Technology, 76131 Karlsruhe, Germany (e-mail: max.voehringer@kit.edu; manfred.thumm@kit.edu; john.jelonnek@kit.edu).

Alexander Marek is with the Fraunhofer Institute for High Frequency Physics and Radar Techniques FHR, 53343 Wachtberg, Germany (e-mail: alexander.marek@fhr.fraunhofer.de).

Stefan Illy, Benjamin Ell, Lukas Feuerstein, Gerd Gantenbein, Tobias Ruess, and Chuanren Wu are with the Institute for Pulsed Power and Microwave Technology, Karlsruhe Institute of Technology, 76131 Karlsruhe, Germany.

Color versions of one or more figures in this article are available at https://doi.org/10.1109/TPS.2025.3564073.

Digital Object Identifier 10.1109/TPS.2025.3564073

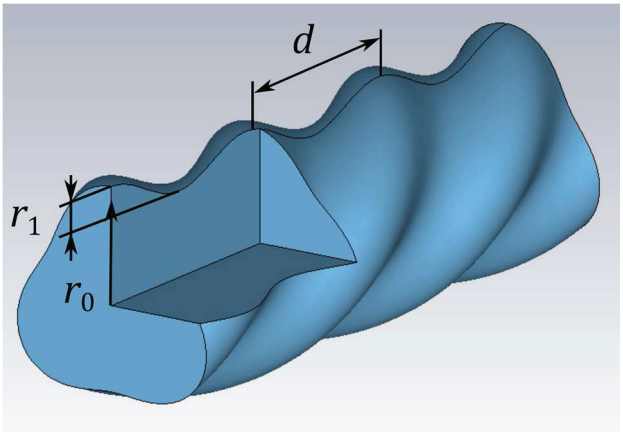

Fig. 1. Vacuum region of a threefold HCIR (m_B = 3) described by (1). The vacuum region is surrounded by copper.

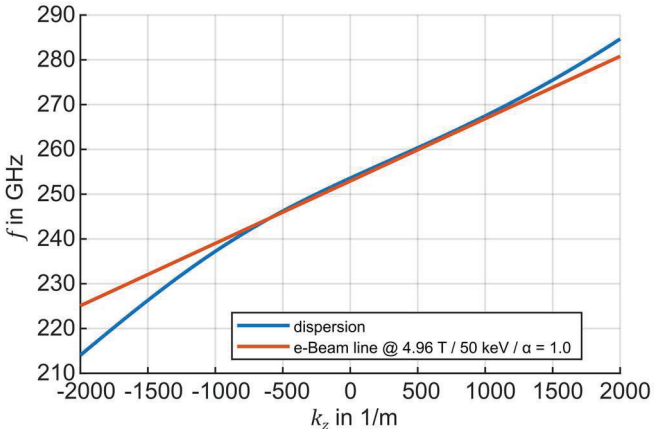

Fig. 2. Dispersion of the HCIR and electron beam line derived from the interaction condition (2).

is prone to manufacturing imperfections, as investigated in this publication.

II. Helically Corrugated Interaction Region

A. Theory

The HCIR utilizes a cylindrical interaction structure with helical corrugations extending in both the azimuthal and axial directions. The radius r is defined by

$$r(\theta, z) = r_0 + r_1 \cos\left(m_B\theta + \frac{2\pi z}{d}\right) \tag{1}$$

in a cylindrical coordinate system. In this expression, r_0 represents the mean radius, r_1 denotes the corrugation amplitude, and d specifies the corrugation period. The parameter m_B indicates the number of corrugations in the azimuthal direction, determining which circular waveguide modes are coupled by the corrugations. The Bragg resonance conditions must be satisfied, requiring that the azimuthal indices m_i of the two coupled modes adhere to $m_1 + m_2 = m_B$. In addition, the wavenumber of mode 2 should approximate $2\pi d$ when mode 1 is near its cutoff frequency [6]. In this study, a HCIR with $m_B = 3$ is employed to couple the $TE_{1,1}$ and $TE_{2,1}$ circular waveguide modes, which rotate in opposite directions. This configuration offers advantages over higher m_B values, such as eliminating the need for an additional mode converter. The fundamental $TE_{1,1}$ circular waveguide mode can be used directly at both the input and output. Furthermore, smaller diameters reduce mode competition significantly. A 3-D representation of the vacuum region for an $m_B = 3$ is shown in Fig. 1.

An axis-encircling electron beam, also known as a large orbit beam, is used. This beam is formed when electrons pass through a cusp in a static magnetic field [8], [9]. Energy transfer from the electron beam to the microwave occurs when the resonance condition [10]

$$\omega \approx s\omega_c + k_z v_z \tag{2}$$

is satisfied. In this context, ω represents the angular frequency of the microwave, ω_c is the electron resonant frequency, s denotes the harmonic number, k_z is the axial wavenumber, and v_z is the axial velocity of the electrons.

B. HCIR at 265 GHz

The gyro-TWA is designed to operate at a target center frequency of 265 GHz, necessitating optimization of the HCIR for this frequency. As a first step, the phase difference between an electron traveling with known parameters and unaffected by any microwave and the electric field vector of the microwave at the end of the interaction region is calculated. To achieve this, the dispersion properties of the HCIR must be determined. This is accomplished by applying a coordinate transformation to "unwrap" the HCIR, eliminating its z-dependence, and simplifying the problem from 3-D to 2-D. Subsequently, a 2-D vector finite-element method [11] is employed to determine the dispersion characteristics of the HCIR's eigenmodes.

The dispersion curve and the electron beam line, derived from the right side of (2), are plotted in the dispersion diagram shown in Fig. 2. Using the frequency offset, the total length of the HCIR, and the time required for an electron to traverse the HCIR, the phase difference at the end of the HCIR can be calculated. This phase difference must remain below π to ensure that the bunched electrons stay within the deceleration phase. If they enter the acceleration phase, over-bunching occurs, causing the microwave to transfer energy back to the electron beam.

The chosen parameters for the HCIR are then verified via PIC simulations with CST Microwave Studio. At 265 GHz, the determined parameters for the HCIR are r_0 = 0.544 mm, r_1 = 0.08 mm and d = 1.16 mm. The overall length of the HCIR is $32d$. To avoid reflections, two cosine tapers with a length of $3d$ are placed at the transitions from HCIR to circular waveguide. For these parameters, an electron beam with an energy of 50 keV, current of 0.6 A, and a pitch factor $\alpha = v_t/v_z$, the ratio between transversal velocity v_t and axial velocity v_z, of 1.0 in a static axial magnetic field of 4.96 T, interacts with the microwave. The achieved maximum gain is 31 dB with a 3 dB bandwidth of 24.6 GHz.

III. Tolerances for Uniform Deviations

A. Deviation in the Dispersion Diagram

As depicted in Fig. 1, the outer shape of the waveguide is quite intricate and not manufacturable by standard processes.

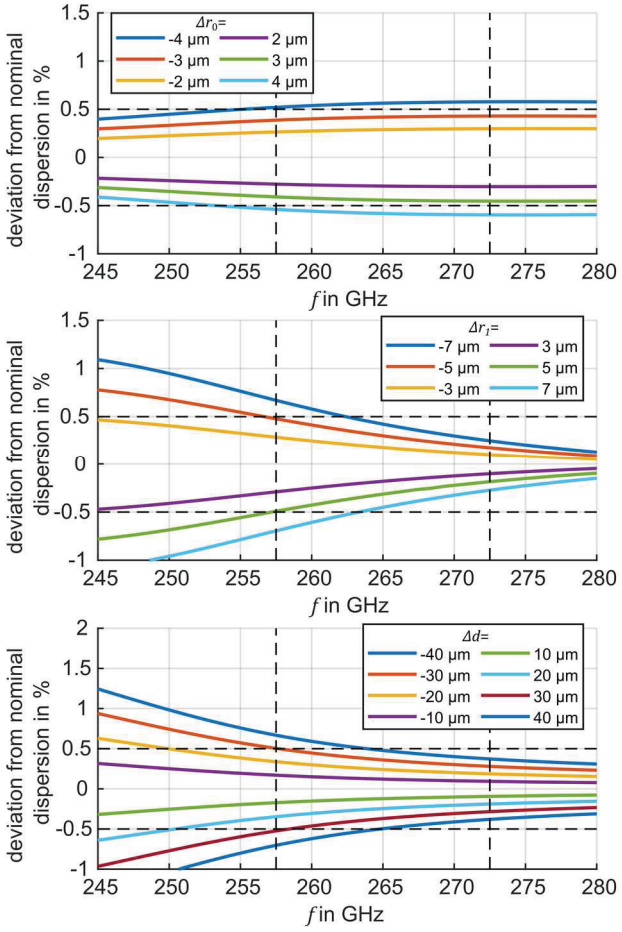

Fig. 3. Relative deviation from the nominal dispersion for different offsets in the HCIR parameters Δr_0 (top), Δr_1 (middle), and Δd (bottom). The acceptable window of operation is indicated by the dashed lines. Here, the relative deviation from nominal dispersion should be limited to $\pm 0.5\%$ in a bandwidth of 15 GHz around a center frequency of 265 GHz.

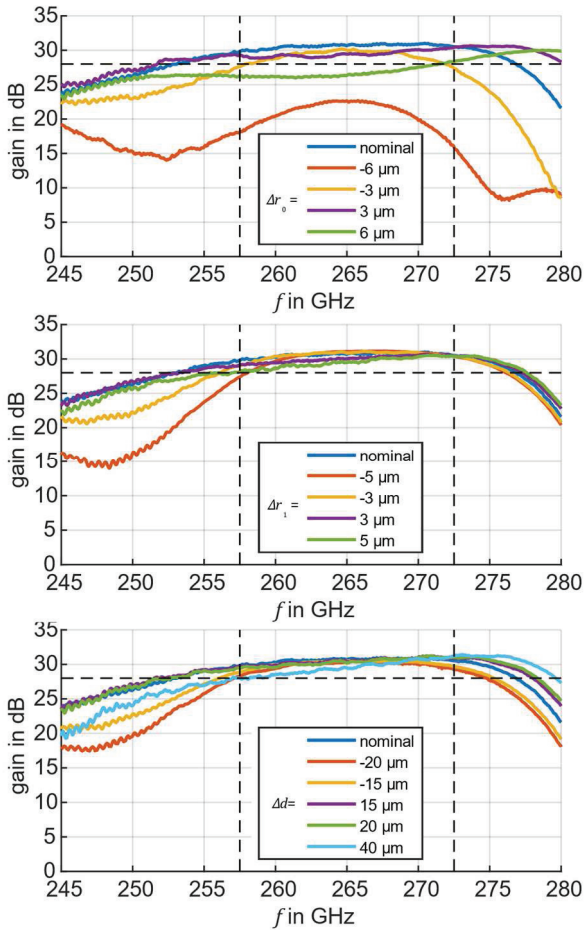

Fig. 4. Influence of distortions on the gain and bandwidth of interaction for different offsets in the HCIR parameters Δr_0 (top), Δr_1 (middle), and Δd (bottom). The acceptable window of operation is indicated by the dashed lines. Here, the gain should be above the 3 dB line (horizontal dashed line) in a bandwidth of 15 GHz around a center frequency of 265 GHz.

In [12], the manufacturing is achieved by first milling an aluminum mandrel in the shape of the vacuum region, which is then electroplated with copper. Finally, the aluminum mandrel is chemically dissolved. This leaves a waveguide with the desired surface structure. However, during every manufacturing process, certain deviations from the nominal geometry are occurring, which require the definitions of tolerances.

The first approach to derive tolerances is to limit the acceptable relative deviation from the nominal HCIRs dispersion in the dispersion diagram to $\pm 0.5\%$, as presented in [12]. Therefore, the dispersion diagram is calculated by using the methodology during the optimization and presented in [11]. The radius definition (1) is adjusted to include deviations Δr_0, Δr_1, and Δd, which results in

$$r(\theta, z) = r_0 + \Delta r_0 + (r_1 + \Delta r_1) \cos\left(m_B \theta + \frac{2\pi z}{d + \Delta d}\right). \quad (3)$$

By adjusting Δr_0, Δr_1, and Δd different dispersions are derived, and the relative deviation compared to the nominal dispersion is calculated. The results are presented in Fig. 3. The relative deviation from nominal dispersion should be limited to $\pm 0.5\%$ in a bandwidth of 15 GHz around a center frequency of 265 GHz. This results in tolerance limits for each parameter, namely $\Delta r_0 = \pm 3\ \mu$m for the mean radius, $\Delta r_1 = \pm 5\ \mu$m for the corrugation amplitude, and $\Delta d = \pm 30\ \mu$m for the corrugation period. Especially, the tolerances for the mean radius Δr_0 and corrugation amplitude Δr_1 are challenging to achieve over the entire length of the HCIR.

B. PIC Simulation of Uniform Deviations

To verify the results in the previous section, PIC simulations with CST Microwave Studio are conducted. Here, the deviations from the nominal HCIR parameters are uniform over the entire length of the HCIR. The mesh cell size is 24 μm in x-, y-, and z-dimension, respectively, and therefore comparable or larger to the size of the deviations, which should be investigated. However, a perfect boundary approximation is implemented in CST Microwave Studio [13]. This allows for good approximation of partially filled cells. The simulation results are depicted in Fig. 4.

To maintain sufficient power over the desired bandwidth, the loss in gain in a 15 GHz band around 265 GHz should not be larger than 3 dB (horizontal dashed line). This results in the tolerance limits for the mean radius of $-3\ \mu\text{m} \leq \Delta r_0 \leq 3\ \mu\text{m}$,

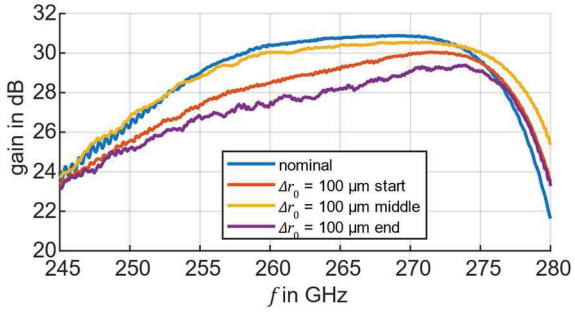

Fig. 5. Influence of a single faulty corruption period at the start, middle (period No. 17), and end of the HCIR.

for the corrugation amplitude of $-5\ \mu\text{m} \leq \Delta r_1 \leq 5\ \mu\text{m}$ and $-20\ \mu\text{m} \leq \Delta d \leq 40\ \mu\text{m}$ for the corrugation period. These values are quite similar to the ones obtained by considering the change in dispersion. Only the tolerances for the corrugation period d are shifted by $+10\ \mu$m. Therefore, defining the tolerances by allowing a $\pm 0.5\%$ deviation in the dispersion diagram is valid. However, this also proves that acceptable tolerances are in the micrometer range and therefore challenging to achieve, even with modern methods.

IV. Tolerances for Nonuniform Deviations

A. Position Dependency of Deviation

In the previous sections, the deviations Δr_0, Δr_1, and Δd are considered uniform along the HCIR. Therefore, they are systematic errors, which can usually be compensated by adjusting the manufacturing process or even by slightly tuning the operation point (acceleration voltage, current, axial magnetic field, and pitch factor). However, the same does not hold true for nonuniform distortions, which cannot be compensated by such measures. In addition, they are very likely to occur during manufacturing, for instance due to vibrations in machine and mandrel. Therefore, their influence, on the interaction between electron beam and microwave is studied. First, the influence of a deviation at a singular position along the HCIR is investigated.

For that, a single larger deviation of $\Delta r_0 = 100\ \mu$m is applied at the starting period, middle period (No. 17 from the start of the HCIR), and final period, respectively. The deviation has a cos-window function, with its maximum at the center of the corrugation. This avoids sharp edges at the contact points of the faulty period with previous and subsequent corrugation.

The results of the PIC simulations are depicted in Fig. 5. The imperfection at the middle period clearly does not deteriorate the HCIR performance strongly, while deviations at the start and end period have a larger effect. The high influence of the end period is to be expected, given the fact that the bunched electron beam transfers most energy in the latter part of the HCIR. Which makes deviations in this area more influential. However, the large influence of the starting period and little effect of the middle period are surprising. They can be explained by the later start of the beam modulation in case of a large deviation at the start of the HCIR, this effectively reduces the interaction region length. While, for a deviation at the middle period, the beam is already modulated and the bunches keep forming even if there is a slight mismatch between the microwave and electron beam.

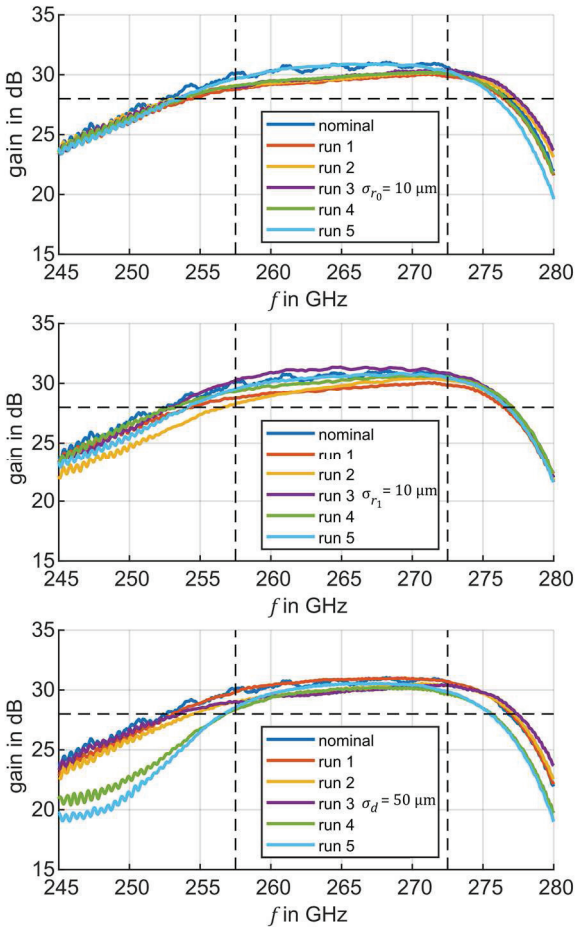

Fig. 6. Influence of Gaussian distributed distortions with the standard deviation σ on the parameters r_0 (top), r_1 (middle), and d (bottom). Each HCIR is created five times with random distributed deviations. The acceptable window of operation is indicated by the dashed lines. Here, the gain should be above the 3 dB line (horizontal dashed line) in a bandwidth of 15 GHz around a center frequency of 265 GHz.

The small effect of the middle period on the performance is a benefit to the manufacturability of the HCIR. During the milling operations, the aluminum mandrel is placed in a fixture. Being fixed at both ends, the force applied by the milling tool cannot distort these parts, and vibrations are less likely to occur; therefore, minimal deviations are expected in these regions. However, the further away from the fixture the milling process takes place, the larger the deformations. Especially in a high aspect ratio workpiece considered here, the highest deviations are therefore most likely to occur toward the middle of the HCIR.

B. Nonuniform Gaussian Distributed Deviations

In practice, the deviations along the HCIR are most likely to be non-uniformly along the HCIR. Caused, for instance, due to vibrations of the mandrel during milling. Therefore, the deviations are assumed to have a Gaussian distribution with a certain standard deviation σ and an average of $\mu = 0$. As a result, the shape of every individual corrugation period is

TABLE I
RESULTING TOLERANCES FOR DIFFERENT APPROACHES

	Uniform deviations		Non-uniform random distributed deviations
	0.5 % deviation in dispersion	**PIC simulation**	
Δr_0	-3 µm $+3$ µm	-3 µm $+3$ µm	$\sigma_{r_0} = 10$ µm
Δr_1	-5 µm $+5$ µm	-5 µm $+5$ µm	$\sigma_{r_1} = 10$ µm
Δd	-30 µm $+30$ µm	-20 µm $+40$ µm	$\sigma_d = 50$ µm

slightly different from its neighbors. Again, to avoid edges in the structure, the deviation of every period has a cos-window with its maximum at the center of each period. As a criterion, the loss in gain has to be less than 3 dB in a frequency band of 15 GHz around the center frequency of 265 GHz. This must hold true for five subsequent simulations, each with newly generated random distributed deviations for all the periods. This is found to hold true for a standard deviation of $\sigma_{r_0} = 10$ μm for the mean radius, $\sigma_{r_1} = 10$ μm for the corrugation amplitude, and $\sigma_d = 50$ μm for the corrugation period. The resulting gain for the HCIRs is plotted in Fig. 6.

Here, the reduction in gain is less than 3 dB in the defined frequency band for every randomly generated HCIR.

All the resulting tolerances from the three different approaches are summarized in Table I. Compared, to the tolerances derived by using uniform deviations along the HCIR as done by using the dispersion diagram and PIC simulations, the standard deviation can be up to a factor three higher compared to the deviations Δr_0 and Δr_1. Therefore, larger deviations can be sustained as long as they only appear localized for the HCIR parameters r_0 and r_1. The parameter d can also sustain larger localized distortions, however, the increase is not substantial.

V. CONCLUSION

This publication presents the interaction region for a helical gyro-TWA at 265 GHz. This includes investigations for acceptable tolerances for the mean radius, corrugation amplitude, and corrugation period. It is found that uniform deviations from the nominal HCIR parameters significantly degrade the gain and bandwidth. This translates to small tolerances in the range of ± 3 μm for the mean radius r_0 and ± 5 μm for the corrugation amplitude r_1. As a result, systematic errors in the manufacturing process need to be compensated. Furthermore, nonuniform deviations are investigated and found to be not as influential, as long as the standard deviation σ is lower than 10 μm for the mean radius r_0 and corrugation amplitude r_1. Therefore, greater deviations can be sustained as long as they are localized. The tolerances during manufacturing are therefore not as stringent if the systematic errors are well compensated, and higher deviations can be tolerated as long as they are nonuniform and randomly distributed.

REFERENCES

[1] A. J. Rossini, A. Zagdoun, M. Lelli, A. Lesage, C. Copéret, and L. Emsley, "Dynamic nuclear polarization surface enhanced NMR spectroscopy," *Acc. Chem. Res.*, vol. 46, no. 9, pp. 1942–1951, Mar. 2013, doi: 10.1021/AR300322X.

[2] K. O. Tan, M. Mardini, C. Yang, J. H. Ardenkjær-Larsen, and R. G. Griffin, "Three-spin solid effect and the spin diffusion barrier in amorphous solids," *Sci. Adv.*, vol. 5, no. 7, p. 1, Jul. 2019, doi: 10.1126/SCIADV.AAX2743.

[3] G. Mathies, S. Jain, M. Reese, and R. G. Griffin, "Pulsed dynamic nuclear polarization with trityl radicals," *J. Phys. Chem. Lett.*, vol. 7, no. 1, pp. 111–116, Dec. 2015, doi: 10.1021/ACS.JPCLETT.5B02720.

[4] T. V. Can, J. J. Walish, T. M. Swager, and R. G. Griffin, "Time domain DNP with the NOVEL sequence," *J. Chem. Phys.*, vol. 143, no. 5, pp. 2–4, Aug. 2015, doi: 10.1063/1.4927087.

[5] W. Jiang et al., "Experimental demonstration of a 10-kW-level G-band gyro-TWT," *IEEE Electron Device Lett.*, vol. 45, no. 5, pp. 905–908, May 2024, doi: 10.1109/LED.2024.3375857.

[6] G. G. Denisov, V. L. Bratman, A. D. R. Phelps, and S. V. Samsonov, "Gyro-TWT with a helical operating waveguide: New possibilities to enhance efficiency and frequency bandwidth," *IEEE Trans. Plasma Sci.*, vol. 26, no. 3, pp. 508–518, Jun. 1998, doi: 10.1109/27.700785.

[7] L. R. Barnett, J. M. Baird, Y. Y. Lau, K. R. Chu, and V. L. Granatstein, "A high gain single stage gyrotron traveling-wave amplifier," in *IEDM Tech. Dig.*, Jul. 1980, pp. 314–317, doi: 10.1109/IEDM.1980.189823.

[8] K. Shinano and H. Itô, "Behavior of a charged particle in a cusp field," *J. Phys. Soc. Jpn.*, vol. 21, no. 9, pp. 1822–1829, Sep. 1966, doi: 10.1143/JPSJ.21.1822.

[9] M. Vöhringer et al., "Universal CUSP-type electron gun for helical gyro-TWTs for DNP-NMR applications," in *Proc. 48th Int. Conf. Infr., Millim., Terahertz Waves (IRMMW-THz)*, Sep. 2023, pp. 1–2, doi: 10.1109/IRMMW-THZ57677.2023.10299143.

[10] S. J. Cooke and G. G. Denisov, "Linear theory of a wide-band gyro-TWT amplifier using spiral waveguide," *IEEE Trans. Plasma Sci.*, vol. 26, no. 3, pp. 519–530, Jun. 1998, doi: 10.1109/27.700786.

[11] S. V. Mishakin and S. V. Samsonov, "Analysis of dispersion and losses in helically corrugated metallic waveguides by 2D vector finite-element method," *IEEE Trans. Microw. Theory Techn.*, vol. 59, no. 9, pp. 2189–2196, Sep. 2011, doi: 10.1109/TMTT.2011.2160201.

[12] C. R. Donaldson, L. Zhang, M. Beardsley, M. Harris, P. G. Huggard, and W. He, "CNC machined helically corrugated interaction region for a THz gyrotron traveling wave amplifier," *IEEE Trans. THz Sci. Technol.*, vol. 8, no. 1, pp. 85–89, Jan. 2018, doi: 10.1109/TTHZ.2017.2778944.

[13] M. C. Balk, C.-S. Chua, X. Li, Y. Alfadhl, and X. Chen, "3D gyrotron simulation with CST STUDIO SUITE," in *Proc. IEEE Int. Vac. Electron. Conf. (IVEC)*, Apr. 2015, pp. 1–3, doi: 10.1109/IVEC.2015.7223736.